NIMFEIA

Deliverable D4.1

Report on soft magnetic systems

Project number	101070290
Project name	Nonlinear Magnons for Reservoir Computing in Reciprocal Space
Project acronym	NIMFEIA
Work package	WP4 – Materials and device fabrication
Type	Report
Dissemination level	Public
Lead beneficiary	Johannes Gutenberg University Mainz
Due date of delivery	Month 18

Authors: Gerhard Jakob (JGU), Mathias Kläui (JGU), Robert Frömter (JGU), Katrin Schultheiss (HZDR)

Disclaimer:

The NIMFEIA project has received funding by the European Union's Research and Innovation Programme Horizon Europe under grant agreement No 101070290. However, views and opinions expressed in this document are those of the authors only and do not necessarily reflect those of the European Union. The European Union cannot be held responsible for them.

1. Development of soft magnetic materials for beyond-state-of-the-art in memory computing using spin waves

1.1. Starting point and literature survey

At the right composition range of Nickel-Iron alloys named Permalloy ($Ni_{75\leq x\leq 82}Fe_{100-x}$, Py) the intrinsic magnetostrictions of nickel and iron, which have opposite sign cancel each other. This leads to an unusually soft magnetic material [1] that possesses highly desirable properties such as extremely low magnetostriction, low coercivity, and vanishingly low magnetic anisotropy, making it attractive for a vast range of applications [2–5] and also extremely suitable for the purposes of NIMFEIA. Nevertheless, each application demands for fine tailoring of magnetic and electric properties. Thin films of permalloy are in-plane magnetized by their shape anisotropy but due to nonideal growth conditions, they usually exhibit an additional slight and possibly detrimental uniaxial in-plane anisotropic behavior. The coercivity and anisotropy of permalloy employed for reservoir computing with nonlinear magnons in reciprocal space should be as low as possible. However, low anisotropy and coercivity of permalloy is also highly desirable for anisotropic magnetoresistance (AMR) sensors [6], which are of high interest for detecting and responding to external magnetic fields.

Py films used in industrially produced devices are in most cases prepared by magnetron sputtering due to its high deposition rates, stability, flexibility in terms of materials, achievable film thicknesses down to the sub-nanometer range, and the variety of controllable parameters, such as the plasma power, chamber pressure, sputtering angle, and deposition temperature. The Johannes Gutenberg-University Mainz (JGU) owns an industry compatible Singulus Rotaris sputtering machine that can deposit on 200 mm wafers. Therefore, it is expected that the further upscaling to the 300 mm wafers utilized by the partner GlobalFoundries (GF)is straightforward, in contrast to transferring parameters from the usually small-scale university substrates of size 10x10 mm^2. Materials optimization began based on published results. The Py properties to be tailored are the magnetic anisotropy [2,3,7,8], the coercivity [9,10], the exchange stiffness [11], and the damping constant [12–14]. Among the reported approaches are modifications of the composition (varying the nickel-to-iron ratio [8,15-17] or doping with transition [18], noble [14], and rare-earth [12,19] metals), material-stack variations [20–23] to modify the Py texture and avoid magnetically “dead” interfacial layers, optimization of the deposition [24,10,25] and annealing parameters [7,11], including field annealing [7], tilting the target [8,9], applying external fields during deposition [8,26,27], and the use of textured substrates [28,29] to promote anisotropy. Even though the material has been widely investigated for several decades, the origins of the different sources of anisotropy, including magnetocrystalline and growth-condition-induced anisotropies, are still a topic of intense discussion. Very early theories describe the crystalline anisotropy of permalloy via a simple vector sum of separate atomic moments [30], while recent studies consider atomic orbital hybridization in a variable chemical environment [31] and the associated charge redistribution [16]. The properties of Py can be significantly modified via field annealing, but the mechanism of the effect is still being discussed.

Various mechanisms resulting in uniaxial anisotropy in Py have been proposed, including Fe-Fe pair ordering effects [32], magnetostrictive contributions [33], and defects including vacancies, contaminants, and grain boundaries [34]. A recent study has found that the electrical resistivity of polycrystalline Py films is higher along the hard-axis direction than along the easy axis, which is in agreement with proposals that directional order can induce magnetic anisotropy in Py [27,35]. In addition to inducing anisotropy, studies have also investigated ways to suppress it:

while Py films that are magnetically shielded during deposition still demonstrate a residual anisotropy [36], annealing in a rotating field is reported to fully suppress the anisotropy but is accompanied by an increase in the film coercivity [7,26]. Rotating the sample during deposition with respect to a tilted target drastically decreases both the coercivity and the anisotropy but only down to a certain plateau [27]. Finally, Py deposition at normal incidence in a rotating external field of 3 mT has been reported to result in isotropic properties when averaging over the entire film [26]; however, these films still exhibit anisotropy on a local scale, as can be concluded from the observation of magnetization ripples on a scale of 100 µm. All the above-mentioned approaches to the minimization of magnetic anisotropy rely on obtaining polycrystalline samples with a random orientation of crystallites, so that the local anisotropy averages out and the samples do not exhibit a net anisotropy [37,38]. However, fcc metals have a tendency to develop a (111) texture to minimize the surface energy, resulting in an intrinsic compressive stress due to the incorporation of surface atoms in the film caused by the high adatom energy [39]; this is also linked to a higher density and lower roughness and coercivity of the resulting films [9,25,40].

To summarize, a range of different factors impact the anisotropy of thin polycrystalline Py films and other magnetic thin films and while the anisotropy of Py can be reduced, residual sources of anisotropy often remain, which can be detrimental for device performance, calling for further approaches to growth optimization. Furthermore, it is of paramount importance that robust techniques are established that can reliably benchmark the influence of varied deposition conditions on the film quality. Since extended thin films frequently contain macroscopic defects that occur randomly and are not necessarily directly related to the specific growth conditions, it is vital that such films are characterized in such a manner that the properties are not dominated by such extrinsic random defects but, rather, reflect the intrinsic properties of the varied deposition parameters. This approach can also be of interest for optimizing the growth conditions and analyzing the magnetic properties of soft magnetic films other than Py.

1.2. Strategy and Methods

Within the requirements of NIMFEIA and based on the literature research, we prepare sets of thin Py films exhibiting in-plane magnetization with varied deposition methods and parameters and investigate them by analysis techniques that probe the films both globally and locally. In addition, we employ lithographic patterning in order to isolate and distinguish the impact of individual sparsely distributed defects. In this manner, we develop an approach to robustly determine the film properties, so that we can reliably extract the influence of the growth procedure, independent of the presence of random macroscopic defects in the films that can otherwise dominate the properties. We then employ this approach to investigate various methods to reduce the coercivity and effectively control the anisotropy of the deposited films, in particular via the application of rotating magnetic fields during growth. This approach can be of interest for optimizing the growth conditions and analyzing the magnetic properties of various thin in-plane magnetic films.

Several sets of samples are produced by room-temperature dc magnetron sputtering in a Singulus Rotaris sputtering system using 10-cm-diameter material targets provided by Singulus on thermally oxidized (001) p-doped silicon substrates with a 100-nm oxide layer placed close to the rotational axis of the round 8-inch-diameter sample holder. Single deposition parameters are systematically varied while keeping the other ones fixed (deposition power in the range 200–1200 W, chamber pressure in the range $4 \times 10^{-3} – 6 \times 10^{-3}$ mbar, or different applied magnetic field protocols). In order to improve the (111) texture of the films, a $Ni_{47}Cr_{42}Fe_{11}$ seed layer is used [41].The complete material stack includes a 4-nm $Ni_{47}Cr_{42}Fe_{11}$ seed layer, on top

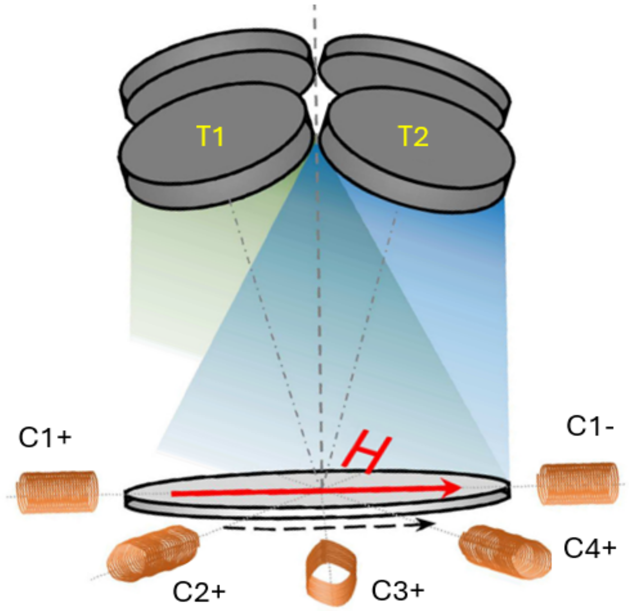

Figure 1: (Modified from [A])

A schematic illustration of the deposition geometry in the Singulus Rotaris sputtering chamber that is used for the Py-thin-film deposition. The sample is placed on a rotating holder and four pairs of coils (C1–C4) are fixed in space in the plane of the holder to generate a magnetic field that is either static and thus rotating in the reference frame of the sample (RMF) or synchronized with the rotation of the sample and thus constant (aligning) in the frame of the sample (AMF).

of which 30 nm of Py ($Ni_{81}Fe_{19}$) is deposited – sufficient to provide a measurable change of the magnetic parameters for the different samples and to minimize the impact of interfacial effects such as intermixing that may dominate the properties of thinner films. Finally, a 4-nm Ta capping layer is deposited to prevent oxidation. The $Ni_{47}Cr_{42}Fe_{11}$ and Ta layers are in all cases deposited under the same conditions (800 W and $P_{Ar} = (3.6 \pm 0.3) \times 10^{-3}$ mbar for the $Ni_{47}Cr_{42}Fe_{11}$ seed layer and 200 W and $P_{Ar} = (3.5 \pm 0.2) \times 10^{-3}$ mbar for the Ta capping), with all layer thicknesses controlled by x-ray reflectometry (XRR). Two different field protocols are investigated, either an "aligning" magnetic field (AMF) that is fixed in space with respect to the rotating sample coordinate frame or a "rotating" magnetic field (RMF) that is fixed in the laboratory frame and therefore rotates with respect to the frame of reference of the film. While sputtering the Py and $Ni_{47}Cr_{42}Fe_{11}$ films, rotating or aligning magnetic fields up to 5 mT are generated by four pairs of sinusoidally commutated solenoids placed in vacuum around the sample holder. A third set of samples is prepared without applying an additional magnetic field (zero magnetic field, ZMF). The deposition tilt is 14° with respect to the substrate normal and the target-to-substrate distance is 20 cm (Fig. 1). During deposition, the sample stage is rotated around its axis at a frequency of 1 Hz to provide uniformly thick films, to remove the influence of static background magnetic fields such as that of the Earth and the stray field of the cathode magnets, as well as to avoid self-shadowing [42].

Another set of samples is deposited by thermal evaporation in an ultrahigh-vacuum (UHV) molecular-beam epitaxy chamber on the same substrates, cooled down to liquid-nitrogen temperatures (no seed layer, 52 nm of Py capped with 4 nm of Au) or at room temperature (25 nm of permalloy capped with 4 nm of Au). Here, the Py evaporator is tilted by 5° with respect to the substrate normal for comparison.

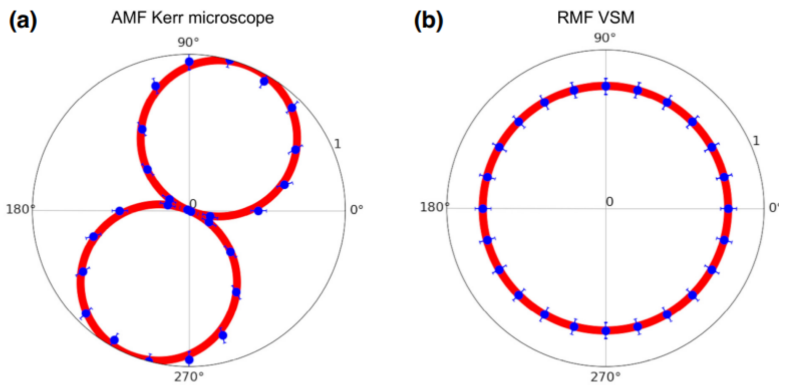

Figure 2: (Modified from [A])

Using aligning magnetic field (AMF) or rotating magnetic field (RMF) option drastically changes the in-plane remnant moment anisotropy.

The magnetic properties of the samples are investigated by both full-field magneto-optical Kerr-effect (MOKE) microscopy utilizing polarized light from a light-emitting diode (LED) (field of view 340 × 450 μm^2) and vibrating sample magnetometry (VSM) (Fig. 2). For investigating the anisotropy, magnetic hysteresis loops are recorded for different in-plane rotation angles of the sample with respect to the external magnetic field direction using a step size ranging from 5° to 15°. To determine the directions of the easy and hard axes, the remanent magnetization versus angle plot is fitted with a function representing the modified Stoner-Wohlfarth model. The anisotropy constant is calculated from the easy- and hard-axis hysteresis loops [43].

The roughness and average particle size of the samples are measured by atomic force microscopy (AFM), XRR, and x-ray diffraction (XRD). The average crystallite size is obtained using the Scherrer formula to describe the broadening of the Py (111) XRD peak. Subsequent patterning of the films into a hexagonal lattice (5 × 5 mm) of disks with 80-µm diameter and 10-µm spacing is performed using near-ultraviolet photolithography and ma-P 1215 positive photoresist, which requires 30 s of soft baking at 90 °C, followed by Ar ion-beam etching at 300 V.

1.3. Results

A first set of Py films is sputtered at room temperature with different adatom energies by varying the sputtering power and chamber pressure, using an external in-plane RMF of 5 mT. For samples with varied sputtering power, the chamber pressure is fixed at 4×10^{-3} mbar and for samples with varied chamber pressure, the sputtering power is fixed at 1200 W. The sputtering rate has a very prominent linear dependence on the deposition power and is only slightly affected by the chamber pressure within the investigated region [Fig. 3(a)]. The Scherrer crystallite size is found to vary significantly and it does not simply follow the adatom energy: the crystallite size increases on lowering the deposition power, which is associated with lowering adatom energies; but it also increases on lowering the Ar pressure, which is associated with higher adatom energies. The AFM data on the average grain size demonstrate a similar trend to the Scherrer crystallite size obtained with XRD. The rms roughness of all samples, obtained from

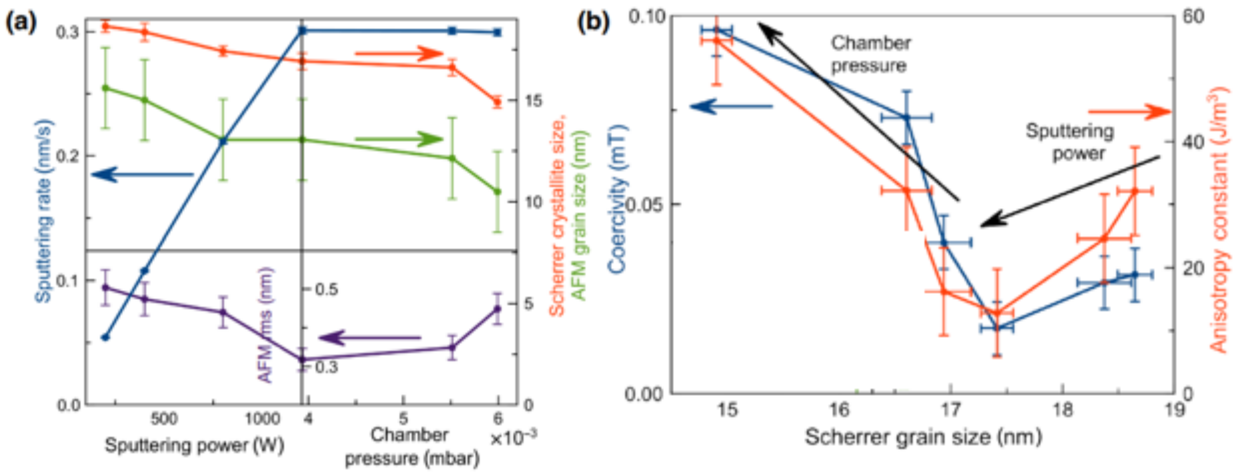

Figure 3: (Modified from [A])

(a) The sputtering rates (blue dots), Scherrer average crystallite sizes (red dots), AFM average grain sizes (green dots), and AFM RMS surface roughness (purple dots) of Py films sputtered with different powers and chamber pressures. For varied sputtering power, the chamber pressure is fixed at 4×10^{-3} mbar and for varied chamber pressure, the sputtering power is fixed at 1200 W. (b) The coercivity (blue dots), anisotropy (red dots), and resistivity (green dots) of the continuous Py films as a function of the Scherrer average crystallite size for growth with a rotating magnetic field (i.e., fixed in the laboratory frame) of 5 mT changes the in-plane remnant moment anisotropy.

5×5 µm^2 AFM scans, is also presented in Fig. 3(a). The magnetic properties of the resulting continuous films, obtained locally using Kerr microscopy and integrating over the whole field of view, are given in Fig. 3(b) versus the average crystallite size obtained from XRD. Both the anisotropy and coercivity of the Py films decrease simultaneously with increasing adatom energy, upon either increasing the sputtering power or lowering the chamber pressure. The combined effect of low inert gas pressure and high deposition power resulting in high deposition rates enables low coercivity and anisotropy values of the 30-nm-thick Py films sputtered in an RMF, down to 0.01 mT and 18 J/m^3, respectively.

All samples demonstrate a small but finite anisotropy constant despite the expected disorienting effect of sputtering on the rotating substrate and in a rotating magnetic field to eliminate anisotropy. Rotating magnetic fields in combination with normal incidence of material flow have been reported [26] to produce magnetically isotropic Py films. This discrepancy might be caused by utilizing the $Ni_{47}Cr_{42}Fe_{11}$ seed layer, a tilted sputtering target orientation, or a different method and/or spatial resolution for determining the magnetic properties compared to the cited paper. Sets of Py-film samples sputtered in the absence of a magnetic field (zero magnetic field, ZMF), in a suppressing magnetic field (RMF), or in an AMF (a static magnetic field) are investigated by means of both local Kerr microscopy and integral VSM averaging over the whole sample. The local Kerr measurements demonstrate a finite anisotropy for a ZMF and an RMF with random values and orientations when measured at different spots in the samples.

Various types of magnetic film defects can be sources of local anisotropy. To isolate sparsely distributed sources of stronger anisotropy that could be causing variations of the magnetic

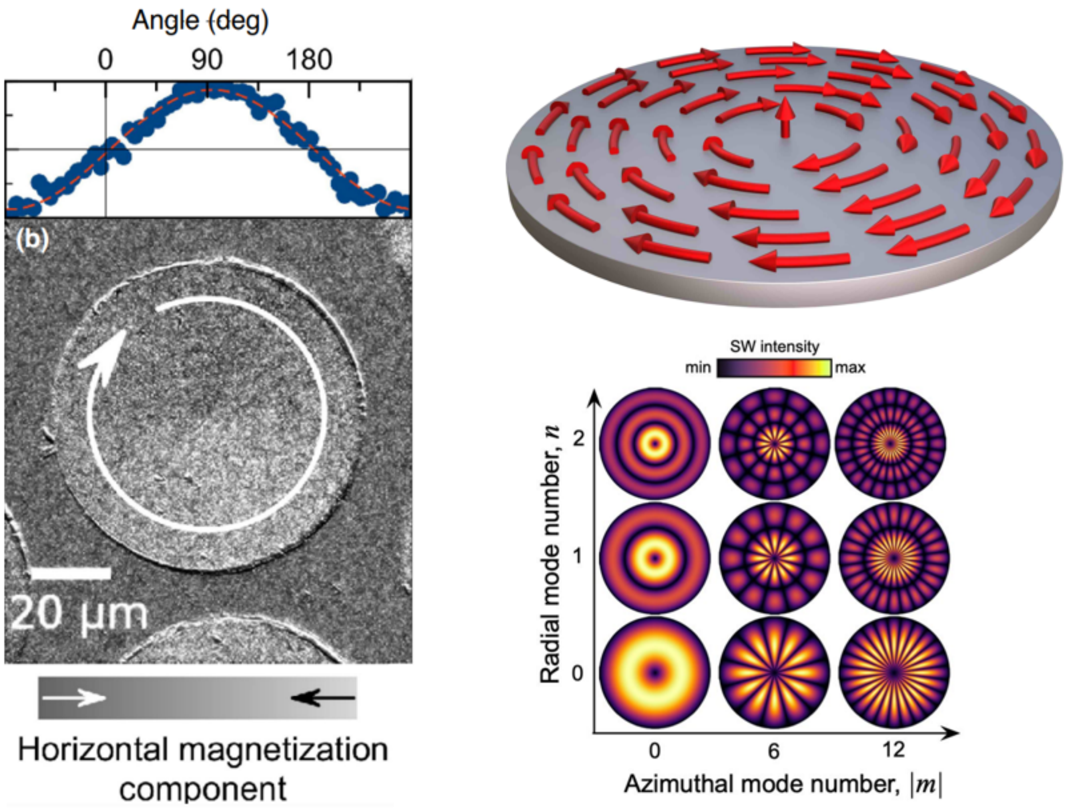

Figure 4: (Left part modified from [A])

Left: Characteristic magnetization configuration of demagnetized Py disks from Kerr microscopy images for rotating-magnetic-field samples displaying the symmetric vortex state. This vortex state is schematically shown in the top right and forms the ground state for the higher order spin wave excitations.

properties in the RMF- and ZMF-sputtered Py films, the films are patterned into hexagonal arrays of disks. Measurements of the angle-resolved coercivity and remanence magnetization on the patterned samples do not exhibit any notable angular $\pi/3$ periodicity, so we can exclude a significant contribution of the dipolar interaction between disks. We observe a discrepancy between the local and averaging measurements of the coercivity and anisotropy of the thin Py films. Patterning into disks results in obtaining uniform local data on magnetic properties, which agrees with the data recorded with averaging methods from a disk array. The choice of averaging over many Py disks improves the signal-to-noise ratio. Measuring single disks free from the mentioned defects multiple times and averaging out over separate measurements results in similar hysteresis curves as for averaging over multiple disks, as long as the individual disk does not carry a defect. Compared to the continuous-film results, the patterned AMF samples retain their easy-axis directions, but the easy-axis hysteresis loops become less square and the hard-axis loops exhibit a higher coercivity when patterned into disks. The hysteresis curves of RMF samples show higher coercivities in all in-plane directions and a completely vanishing anisotropy, which indicates that applying a rotating magnetic field is an effective strategy to further optimize the Py properties. The magnetic states of demagnetized disks are also qualitatively different: AMF Py disks tend to form S states [44] where the magnetization is predominantly aligned with the easy axis, while RMF disks form single vortices with a circular magnetization distribution (Fig. 4) as required for the purposes of NIMFEIA.

1.4. Summary and conclusions

In conclusion, we investigated the effect of varied magnetron sputtering conditions on the magnetic properties of Py, in order to obtain soft magnetic isotropic thin films. The best samples with the lowest coercivity (down to 0.01 mT) and vanishing average anisotropy are obtained using higher sputtering powers (1200 W) and low Ar pressures (4×10^{-3} mbar). The above-discussed approaches are found to improve the magnetic properties of Py by affecting the crystallite size and have been reported to lead to the formation of denser and smoother films. We observe a local variation of the magnetic properties of continuous Py films despite the disorienting effects of sample rotation with respect to the target tilt and the rotating external magnetic field. The patterning of such films into arrays of disks suppresses this variation, which suggests a dominant long-range influence of random defects that affect the magnetic properties of the films in the unpatterned samples. Thus, the investigation of patterned samples provides a general and robust approach to investigate the intrinsic film properties, which can then be unambiguously related to variations in deposition conditions.

The goal to achieve optimized thin films of soft magnetic materials for the applications within NIMFEIA has been achieved.

This report is based largely on the scientific results that are published with NIMFEIA acknowledgements in [A]. There, a more detailed scientific discussion can be found extending also to magnetoresistive effects that are not topic of NIMFEIA, as NIMFEIA relies on the magnetic properties.

2. Publications

[A] **Tailoring Magnetic Properties and Suppressing Anisotropy in Permalloy Films by Deposition in a Rotating Magnetic Field,**
Olga Lozhkina, Fabian Kammerbauer, Maria-Andromachi Syskaki, Aravind Puthirath Balan, Pascal Krautscheid, Mehran Vafaee Khanjani, Jan Kubik, Stephen O'Brien, Robert M. Reeve, Gerhard Jakob, Robert Frömter, and Mathias Kläui,
Phys. Rev. Applied **20**, 014021 (2023), doi: 10.1103/PhysRevApplied.20.014021

3. References

[1] K. Barmak and K. Coffey, *Metallic Films for Electronic, Optical and Magnetic Applications: Structure, Processing and Properties* (Woodhead Publishing, Sawston, Cambridge, UK, 2014).

[2] A. García-Arribas, E. Fernández, A. V. Svalov, G. V. Kurlyandskaya, A. Barrainkua, D. Navas, and J. M. Barandiaran, *Tailoring the magnetic anisotropy of thin film permalloy microstrips by combined shape and induced anisotropies*, Eur. Phys. J. B **86**, 1 (2013).

[3] E. B. Park, S.-U. Jang, J.-H. Kim, and S.-J. Kwon, *Induced magnetic anisotropy and strain in permalloy films deposited under magnetic field*, Thin Solid Films **520**, 5981 (2012).

[4] B. Borie, J. Wahrhusen, H. Grimm, and M. Kläui, *Geometrically enhanced closed-loop multi-turn sensor devices that enable reliable magnetic domain wall motion*, Appl. Phys. Lett. **111**, 242402 (2017).

[5] D. A. Allwood, G. Xiong, C. Faulkner, D. Atkinson, D. Petit, and R. Cowburn, *Magnetic domain-wall logic*, Science **309**, 1688 (2005).

[6] S. Andreev and P. Dimitrova, *Anisotropic-magnetoresistance integrated sensors*, J. Optolectron. Adv. Mater. **7**, 199 (2005).

[7] T. Iwata and F. Hagedorn, *Annealing behavior of induced anisotropy and related magnetic properties in permalloy films*, J. Appl. Phys. **40**, 2258 (1969).

[8] D. O. Smith, *Anisotropy in permalloy films*, J. Appl. Phys. **30**, S264 (1959).

[9] M. Kateb, H. Hajihoseini, J. T. Gudmundsson, and S. Ingvarsson, *Comparison of magnetic and structural properties of permalloy $Ni_{80}Fe_{20}$ grown by dc and high power impulse magnetron sputtering*, J. Phys. D: Appl. Phys. **51**, 285005 (2018).

[10] M. Sultan, *Effect of gas pressure and flow rate on the plasma power and deposition rate in magnetron sputtering system*, Res. J. Nanosci. Eng **2**, 1 (2018).

[11] J. Wei, Z. Zhu, C. Song, H. Feng, P. Jing, X. Wang, Q. Liu, and J. Wang, *Annealing influence on the exchange stiffness constant of permalloy films with stripe domains*, J. Phys. D: Appl. Phys. **49**, 265002 (2016).

[12] C. Luo, Z. Feng, Y. Fu, W. Zhang, P. Wong, Z. Kou, Y. Zhai, H. Ding, M. Farle, and J. Du, et al., *Enhancement of magnetization damping coefficient of permalloy thin films with dilute Nd dopants*, Phys. Rev. B **89**, 184412 (2014).

[13] Q. Chen, Y. Yin, H. Yuan, X. Zhou, Z. Huang, J. Du, and Y. Zhai, *Effect of dilute rare-earth doping on magnetodynamic properties of permalloy films*, IEEE Magn. Lett. **10**, 1 (2019).

[14] S. Mizukami, T. Kubota, X. Zhang, H. Naganuma, M. Oogane, Y. Ando, and T. Miyazaki, *Influence of Pt doping on Gilbert damping in permalloy films and comparison with the perpendicularly magnetized alloy films*, Jpn. J. Appl. Phys. **50**, 103003 (2011)

[15] R. Bozorth, *The permalloy problem*, Rev. Mod. Phys. **25**, 42 (1953).

[16] L. Yin, D. Wei, N. Lei, L. Zhou, C. Tian, G. Dong, X. Jin, L. Guo, Q. Jia, and R. Wu, *Magnetocrystalline Anisotropy in Permalloy Revisited*, Phys. Rev. Lett. **97**, 067203 (2006).

[17] J. Han-Min, C.-O. Kim, T.-D. Lee, and H.-J. Kim, *Origin of magnetization-induced anisotropy of magnetic films*, Chin. Phys. **16**, 3520 (2007).

[18] J. Rantschler, R. McMichael, A. Castillo, A. Shapiro, W. Egelhoff Jr, B. Maranville, D. Pulugurtha, A. Chen, and L. Connors, *Effect of 3d, 4d, and 5d transition metal doping on damping in permalloy thin films,* J. Appl. Phys. **101**, 033911 (2007)

[19] W. Bailey, P. Kabos, F. Mancoff, and S. Russek, et al., *Control of magnetization dynamics in $Ni_{81}Fe_{19}$ thin films through the use of rare-earth dopants*, IEEE Trans. Magn. **37**, 1749 (2001).

[20] J. Beik Mohammadi, G. Mankey, C. K. Mewes, and T. Mewes, *Strong interfacial perpendicular anisotropy and interfacial damping in $Ni_{0.8}Fe_{0.2}$ films adjacent to Ru and SiO2*, J. Appl. Phys. **125**, 023901 (2019).

[21] Y. Zhao, Q. Song, S.-H. Yang, T. Su, W. Yuan, S. S. Parkin, J. Shi, and W. Han, *Experimental investigation of temperature-dependent Gilbert damping in permalloy thin films*, Sci. Rep. **6**, 1 (2016).

[22] S. Kezilebieke, M. Ali, B. Shadeke, and R. Gunnella, *Magnetic properties of ultrathin $Ni_{81}Fe_{19}$ films with Ta and Ru capping layers*, J. Phys.: Condens. Matter **25**, 476003 (2013).

[23] M. Kowalewski, W. Butler, N. Moghadam, G. Stocks, T. Schulthess, K. Song, J. Thompson, A. Arrott, T. Zhu, and J. Drewes, et al., *The effect of Ta on the magnetic thickness of permalloy ($Ni_{81}Fe_{19}$) films*, J. Appl. Phys. **87**, 5732 (2000).
[24] H. Seet, X. Li, J. Yi, W. Ooi, and K. Lee, *Effect of deposition methods on the magnetic properties of nanocrystalline permalloy*, J. Alloys Compd. **449**, 284 (2008).
[25] A. Kavitha, R. Kannan, and S. Rajashabala, *Effect of target power on the physical properties of Ti thin films prepared by dc magnetron sputtering with supported discharge*, Mater. Sci. Poland **35**, 173 (2017).
[26] E. Fuchs and W. Zinn, *Isotropic permalloy films*, J. Appl. Phys. **34**, 2557 (1963).
[27] M. Kateb, E. Jacobsen, and S. Ingvarsson, *Application of an extended van der Pauw method to anisotropic magnetoresistance measurements of ferromagnetic films*, J. Phys. D: Appl. Phys. **52**, 075002 (2018).
[28] J. Berendt, J. Teixeira, A. García-García, M. Raposo, P. Ribeiro, J. Dubowik, G. Kakazei, and D. Schmool, *Tunable magnetic anisotropy in permalloy thin films grown on holographic relief gratings*, Appl. Phys. Lett. **104**, 082408 (2014).
[29] X. Li, X. Sun, J. Wang, and Q. Liu, *Magnetic properties of permalloy films with different thicknesses deposited onto obliquely sputtered Cu underlayers*, J. Magn. Magn. Mater. **377**, 142 (2015)
[30] L. McKeehan, *Magnetic interaction and resultant anisotropy in unstrained ferromagnetic crystals*, Phys. Rev. **52**, 18 (1937).
[31] D. C. Rodrigues, A. B. Klautau, A. Edström, J. Rusz, L. Nordström, M. Pereiro, B. Hjörvarsson, and O. Eriksson, *Magnetic anisotropy in permalloy: Hidden quantum mechanical features*, Phys. Rev. B **97**, 224402 (2018).
[32] S. Chikazumi, *Ferromagnetic properties and superlattice formation of iron nickel alloys (i)*, J. Phys. Soc. Jpn. **5**, 327 (1950).
[33] J. Slonczewski, *Induced anisotropy in Ni-Fe films*, IEEE Trans. Magn. **4**, 15 (1968).
[34] C. Wilts and F. Humphrey, *Magnetic anisotropy in flat ferromagnetic films: A review*, J. Appl. Phys. **39**, 1191 (1968).
[35] M. Kateb and S. Ingvarsson, *Correlation of uniaxial magnetic anisotropy axes and principal resistivities in polycrystalline ferromagnetic films*, J. Magn. Magn. Mater. **532**, 167982 (2021).
[36] W. Andrä, Z. Málek, W. Schüppel, and O. Stemme, *"Spontaneous magnetic anisotropy" in polycrystalline thin films*, J. Appl. Phys. **31**, 442 (1960).
[37] K. J. Harte, *Theory of large-angle ripple in magnetic films*, J. Appl. Phys. **37**, 1295 (1966).
[38] R. Alben, J. Becker, and M. Chi, *Random anisotropy in amorphous ferromagnets*, J. Appl. Phys. **49**, 1653 (1978)
[39] C. V. Thompson, *Structure evolution during processing of polycrystalline films*, Annu. Rev. Mater. Sci. **30**, 159 (2000).
[40] K. Chan and B. Teo, *Effect of Ar pressure on grain size of magnetron sputter-deposited Cu thin films*, IET Sci., Meas. Technol. **1**, 87 (2007).
[41] W. Lee, M. Toney, and D. Mauri, *High magnetoresistance in sputtered permalloy thin films through growth on seed layers of* $(Ni_{0.81}Fe_{0.19})_{1-x}Cr_x$, IEEE Trans. Magn. **36**, 381 (2000).
[42] P. Solovev, A. Izotov, and B. Belyaev, *Microstructural and magnetic properties of thin obliquely deposited films: A simulation approach*, J. Magn. Magn. Mater. **429**, 45 (2017)
[43] M. Johnson, P. Bloemen, F. Den Broeder, and J. De Vries, *Magnetic anisotropy in metallic multilayers*, Rep. Prog. Phys. **59**, 1409 (1996).
[44] M. Schneider, H. Hoffmann, S. Otto, T. Haug, and J. Zweck, *Stability of magnetic vortices in flat submicron permalloy cylinders*, J. Appl. Phys. **92**, 1466 (2002)